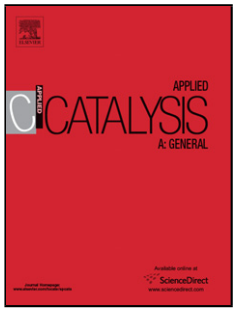

Effect of pretreatment conditions on acidity and dehydration activity of CeO_2-MeO_x catalysts

Muthu Kumaran Gnanamani (Conceptualization) (Methodology) (Investigation), Richard Garcia (Formal analysis) (Investigation), Gary Jacobs (Formal analysis) (Data curation) (Validation) (Writing - review and editing), Kinga Góra-Marek (Formal analysis) (Investigation) (Data curation), Donald C. Cronauer (Investigation)<ce:contributor-role>Reources), A. Jeremy Kropf (Formal analysis)<ce:contributor-role>Data Curation) (Investigation) (Resources), Christopher L. Marshall (Investigation) (Resources)

PII: S0926-860X(20)30315-X

DOI: https://doi.org/10.1016/j.apcata.2020.117722

Reference: APCATA 117722

To appear in: *Applied Catalysis A, General*

Received Date: 24 February 2020

Revised Date: 15 June 2020

Accepted Date: 24 June 2020

Please cite this article as: Gnanamani MK, Garcia R, Jacobs G, Góra-Marek K, Cronauer DC, Kropf AJ, Marshall CL, Effect of pretreatment conditions on acidity and dehydration activity of CeO_2-MeO_x catalysts, *Applied Catalysis A, General* (2020), doi: https://doi.org/10.1016/j.apcata.2020.117722

Effect of pretreatment conditions on acidity and dehydration activity of CeO_2-MeO_x catalysts

Muthu Kumaran Gnanamani[a*], Richard Garcia[b], Gary Jacobs[b,c], Kinga Góra-Marek[d], Donald C. Cronauer[e], A. Jeremy Kropf[e], Christopher L. Marshall[e]

[a] Center for Applied Energy Research, University of Kentucky, 2540 Research Park Drive, Lexington, KY 40511, USA

[b] Department of Chemical Engineering and Biomedical Engineering, UTSA, One UTSA Circle, San Antonio, TX 78249, USA

[c] Department of Mechanical Engineering, UTSA, One UTSA Circle, San Antonio, TX 78249, USA

[d] Department of Chemistry, Jagiellonian University in Krakow, 2 Gronostajowa St., 30-387 Krakow, Poland

[e] Argonne National Laboratory, Argonne, IL 60439, USA

[*]Corresponding author: Tel: +1 859-257-0240

Email address: muthu.gnanamani@uky.edu (MK Gnanamani)

Graphical abstract

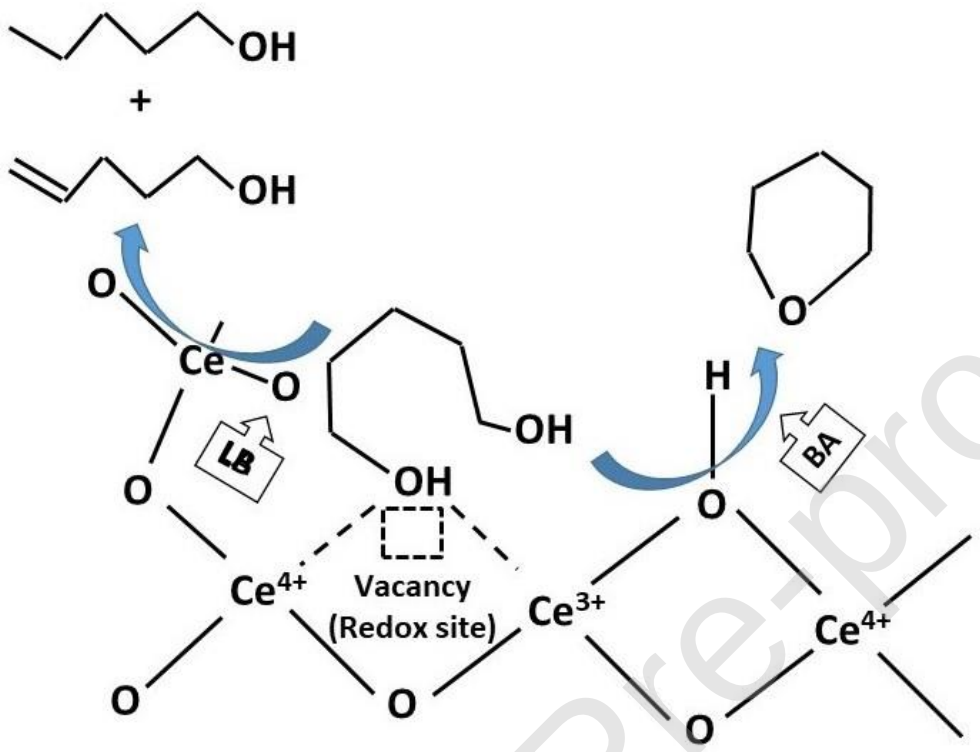

Highlights

- Metal oxide was added to modify the acid-base characteristics of ceria
- Pretreatment conditions (H_2, air) has a profound effect on both redox and acid-base functions of ceria
- B and L acidity were correlating with 1,5-pentanediol or cyclohexanol conversion
- Oxygen vacancies in conjunction with acid-base sites control the dehydration selectivity
- H_2-treatment seems more favorable than air-pretreatment to achieve higher conversion and selectivity

Abstract

A series of MeO_x-modified CeO_2 (CeO_2-MnO_x, CeO_2-ZnO, CeO_2-MgO, CeO_2-CaO, and CeO_2-Na_2O) catalysts were prepared by the impregnation of CeO_2 with corresponding metal nitrates. Acidity and oxidation state of cerium were investigated on both oxidized and reduced catalysts by employing Fourier Transform Infrared spectroscopy (FTIR) on adsorbed pyridine and *in situ* H_2-Temperature Programmed Reduction/X-ray Absorption Spectroscopy (H_2-TPR/XAS) techniques, respectively. Metal oxide addition tended to alter both type and number of acid sites on ceria. EXAFS data showed a significant difference in N_{Ce-O} between unmodified and MeO_x-CeO_2, suggesting that added MeO_x interferes with vacancy formation on ceria during reduction. In comparison with air-pretreated samples, H_2-pretreated ones under similar conversion of 1,5 pentanediol exhibited a higher selectivity towards linear alcohols. Alcohol conversion found to correlate with total acidity (i.e., Brønsted and Lewis). CeO_2 benefited from the addition of alkali (Na) or alkaline earth metals (Mg, Ca) by producing unsaturated alcohols.

Keywords: Dehydration; CeO_2-MeO_x; 1,5-pentanediol; X-ray Absorption Spectroscopy; Acidity

1. Introduction

Metal oxides are known to catalyze dehydration reactions [1-5]. The selectivity of dehydration is often hampered by many side products originating from reactions such as dehydrogenation, dehydrocyclization, and dimerization. In general, preparation and pretreatment conditions of metal oxides have played a significant role in modifying the activity and selectivity of dehydration and other acid-catalyzed reactions [6]. Alumina and zirconia are considered to be highly selective dehydration catalysts, but they can still produce a wide range of products if subjected to different pretreatment conditions [7-9]. Several mixed metal oxides, such as SiO_2-Al_2O_3 [10], CeO_2-ZrO_2 [11], and ZrO_2/SiO_2 [12], were tested as dehydration catalysts with the aim

of modifying their acid-base function, which in turn controls catalyst activity and product selectivity. Viter and Nagornyi [13] studied SnO_2/B_2O_3 binary oxides as solid catalysts for dehydration of 2-methyl-3-butyn-2-ol (MBOH) and the authors found that dehydration activity of SnO_2/B_2O_3 was close to that of ZrO_2/SiO_2.

CeO_2 is a well-known oxygen storage material used in three-way catalytic converters [14]. Apart from redox chemistry, CeO_2 also possesses mild acidity and significant basicity, found to be effective for carrying out many organic transformations, including dehydration [14-18]. When CeO_2 is pretreated at elevated temperatures and/or exposed to reducing conditions, oxygen vacancies and other reduced defect sites (e.g., bridging OH groups) are formed, accompanied by a change in the oxidation state of ceria from Ce^{4+} to Ce^{3+} [19]. On the other hand, under oxidizing conditions, CeO_2 surfaces can be terminated by O or OH groups [20]. This degree of coordinative unsaturation at the surface influences the nature of intermediates formed upon adsorption of alcohols. For instance, primary alcohols favor dehydrogenation over dehydration on oxidized CeO_2 (111) while reduced CeO_x (111) surfaces yield more olefins (i.e., dehydration) compared to aldehyde (i.e., dehydrogenation) [21]. Mudiyanselage et al. conducted ethanol conversion reactions on CeO_2 and Ru/CeO_2, and the authors [22] found that dehydration to ethylene occurs mainly at about 700 K, with intermediates being ethoxides adsorbed on surface oxygen defect sites of CeO_2. Jacobs and co-workers [23] pointed out the significance of defect sites of CeO_2 on stabilizing the ethoxide intermediate, which in the presence of steam undergoes oxidative dehydrogenation to produce acetate (analogous to formate in methanol steam reforming), with subsequent demethanation resulting in the production of CO_2 during steam reforming of ethanol over metal/CeO_2. In a study by Ohtake et al., hydrothermally developed ceria was shown to have both higher ethanol conversion and ethylene selectivity in comparison with a reference catalyst.

The authors pointed out that higher surface area and Lewis basicity were influential properties of ceria [24]. Zaki and Sheppard [25] evaluated the effects of calcination on the dehydration of 2-propanol using IR spectroscopy, and the authors concluded that higher calcination temperature leads to a higher degree of surface shell reduction of ceria, which decreases electron mobility. This may explain the observed drop in the dehydration activity of ceria.

The Sato group has investigated CeO_2 and other rare-earth oxides (REO's) for the selective dehydration of terminal diols to unsaturated alcohols [26-31]. The latter compounds find many applications within the fine chemicals industry. The authors have shown that CeO_2 produces unsaturated alcohol selectively from 1,3-butanediol, while a mixture of products forms using 1,5-pentanediol (i.e., a terminal diol). The authors argued that differences in the carbon chain length between these two alcohols could cause the respective intermediate to be stabilized on the catalytic sites of CeO_2. In our previous work [32], we reported that Na acts as an acid-base moderator for CeO_2, allowing control of the product selectivity from 1,5-pentanediol. This leads us to believe that surface modification of CeO_2 by adding another oxide [33] may avail an entirely different chemistry that might have an impact on both conversion and product selectivity for dehydration of 1,5-pentanediol.

Thus, in this contribution, we investigate the influence of pretreatment conditions (air or H_2) of CeO_2 and MeO_x-modified CeO_2 catalysts on the dehydration of 1,5-pentanediol reaction to better understand the role of oxygen vacancies in addition to acid sites present on the surface of activated CeO_2, with the aim of controlling both conversion and selectivity. The acidity was measured using FTIR of adsorbed pyridine. *In situ* H_2-Temperature Programmed Reduction X-ray Absorption Near-Edge Spectroscopy and Extended X-ray Absorption Fine Structure (H_2-TPR XANES/EXAFS) were utilized for the analysis of partially reduced cerium in CeO_2. The reaction

of cyclohexanol - which is considered a tool for measuring acidity and basicity of metal oxides – was carried out on all catalysts after subjecting them to reducing or oxidizing conditions. Results from the dehydration of 1,5-pentanediol on CeO_2 and MeO_x-modified CeO_2 catalysts suggests that, irrespective of the pretreatment conditions, total acidity correlates with catalytic activity but that selectivity to linear alcohols varies depending on the nature of the MeO_x added, as well as the catalyst pretreatment conditions.

2. Experimental

2.1. Sample preparation

In this work, CeO_2-MeO_x (90Ce:10Me) catalysts (CeO_2-MnO_x, CeO_2-ZnO, CeO_2-MgO, CeO_2-CaO, and CeO_2-Na_2O) were prepared by incipient-wetness impregnation using respective metal nitrates and commercially available CeO_2. More details can be found in our earlier publication [33]. CeO_2 was purchased from Rhodia, and had a high surface area of 114 cm^2/g. All metal nitrates [manganese (II) nitrate hydrate 98%, zinc (II) nitrate hexahydrate 98%, magnesium (II) nitrate hexahydrate 98%, calcium (II) nitrate tetrahydrate 99.9%, and sodium (I) nitrate 99.9%] were purchased from Sigma Aldrich and used as is, without further purification. Briefly, the required metal nitrates were dissolved in deionized water and added to previously weighed CeO_2 to produce a Ce to Me ratio of 90:10. The samples were then dried in an air oven held at 120 °C overnight and finally calcined in a muffle furnace at 500 ℃ for 4 h. For the purpose of comparison, pure CeO_2 was subjected to similar treatments as described above, excluding the metal nitrate addition.

2.2. Characterization

The catalyst acidity was determined by FTIR pyridine adsorption using a Bruker Vertex 70 spectrometer equipped with an MCT detector with a spectral resolution of 2 cm^{-1}. The catalyst

sample was pressed into a self-supporting disc (3.5 cm^2; ca.15 mg/cm^2) and pretreated *in situ* in an IR cell by flowing either air at 350 ℃ or H_2 at 500 ℃ for one hour. Both temperature and nature of pretreating environment are major factors that influence the surface characteristics of ceria. One hour of pretreatment time is enough for characterization to attain the reduced or oxidized state of CeO_2. After outgassing at the same temperature, the sample was cooled to 130 ℃ prior to contacting with pyridine (>99.8%, Sigma Aldrich) vapor. The physisorbed pyridine was subsequently removed by evacuation at the same temperature. The Brønsted and Lewis acidity was inferred from the intensities of the 1545 cm^{-1} band for pyridinium ions (PyH^+) and the 1444, 1450 cm^{-1} bands for Py coordinatively bonded to Lewis sites (PyL). The absorption coefficients 0.07 and 0.1 $cm^2/\mu mol$ were used to characterize the Brønsted and Lewis acid sites, respectively [34,35].

H_2-TPR XAFS experiments were performed at the Materials Research Collaborative Access Team (MR-CAT) beamline at the Advanced Photon Source, Argonne National Laboratory. A cryogenically cooled Si (111) monochromator was used to select the incident energy, and a rhodium-coated mirror was used to reject higher-order harmonics of the fundamental beam energy. The experimental setup was as outlined by Jacoby [36]. A stainless-steel multi-sample holder (4.0 mm i.d. channels) allowed for testing the in-situ reduction of six samples during temperature-programmed heating. The samples were diluted with silica gel at a weight ratio (silica/sample) of approximately 5. Approximately 6 mg of each sample was loaded as a self-supporting wafer in each channel. The holder was placed in the center of a quartz tube, equipped with gas and thermocouple ports and Kapton windows. The amount of sample used was optimized for the Ce L_3 edge (5723 eV). The quartz tube was placed in a clamshell furnace mounted on a positioning table. Each sample cell was positioned relative to the beam by finely adjusting the position of the

table to an accuracy of 20 μm for repeated scans. Once the sample positions were fine-tuned, the reactor was purged with helium for more than 5 min at 30 ml/min. Then, the reactant gas (3.5% H_2/He) was flowed through the samples (95 ml/min), and a temperature ramp of ~1.8 °C/min was initiated for the furnace. The final temperature was ~975 °C, and it was held for ~45 min. The Ce L_3-edge spectra were recorded in transmission mode, and a Cr metallic foil spectrum was measured simultaneously with each sample spectrum for energy calibration. Data reduction of the XAFS spectra was carried out using the WinXAS program [37], and raw data were processed to give the normalized XANES spectra. Linear combination fitting of spectra with appropriate reference compounds was carried out. The initial spectrum of each catalyst was used as a fingerprint for the Ce^{4+} oxidation state, while the final spectrum of a 0.5%Pt/$Ca_{0.50}Ce_{0.50}O_X$ catalyst following TPR (30 ml/min of 4%H_2/He, 820 °C, 1.5 h hold time) from [38] was used as a fingerprint of the Ce^{3+} oxidation state for all samples, since its lineshape resembled Ce^{3+} compounds, such as $Ce(NO_3)_3$ or $Ce(Cl_3)_3$. EXAFS data reduction and fitting were carried out using the WinXAS program [see above], Atoms [39], FEFF [40], and FEFFIT [40] programs. The k- and r-ranges were chosen to be approximately $\Delta k = 2.5 - 10$ $Å^{-1}$ and $\Delta R = 1.0 - 2.5$ Å, respectively.

2.3. Catalytic reaction

The dehydration of 1,5-pentanediol or cyclohexanol was carried out in a fixed-bed flow reactor under an atmosphere of N_2 (air pretreated) or H_2 (H_2 pretreated) at a flow rate of 50 cm^3 min^{-1}. The reactor was a stainless-steel tube having a length of 35.6 cm with an internal diameter of 0.9 cm. The total catalyst bed length would be approximately 2.5 cm for 1.0 g of catalyst sample (40-100 microns) mixed with an equal amount of the powdered glass beads of similar sizes and fixed between the quartz wool, which acts as a catalyst bed. Before each reaction, the sample was

preheated in the reactor either in airflow (50 cm^3 min^{-1}) at 350 ℃ for two hours or H_2 flow (50 cm^3 min^{-1}) at 500 ℃ for two hours. After the catalyst bed temperature reached to 350 ℃, the alcohol of choice [1,5-pentanediol (0.6 ml/h) or cyclohexanol (3.0 ml/h)] was fed into the reactor along with N_2 or H_2 gas flow (50 cm^3 min^{-1}). The selection of a reaction temperature of 350 °C was based on the literature [27] and the LHSV was chosen to be 0.6 ml/h for 1,5-PDO and 3.0 ml/h for cyclohexanol to achieve a reasonable level of conversion. The liquid products collected periodically in the trap maintained at 5 ℃ were analyzed by gas chromatography using an Agilent 7890 instrument equipped with a DB-5 capillary column and an FID detector. The corresponding FID response factor was applied for each oxygenated material found in the reactor mixture [41]. The products are identified as propanol, tetrahydropyran, tetrahydropyran-2-one, 4-penten-1-ol, 1-pentanol, cyclopentanol, and cyclopentanone, ethanol, 3,4-dihydropyran, 2-methyl cyclopentanone, cyclohexane methanol, 4-penten-1-ol propanoate, valeric acid pentenyl ester, cyclohexane carboxylic acid cyclohexyl ester, and 2,2-dimethyl 3-octanol. As you can see, there are esters with high molecular weights whose formation mechanism is uncertain. This precludes a complete material balance. The effluent gases were collected in a Tedlar gas bag during various time intervals and analyzed using a micro GC (Inficon Fusion) to identify the formation, if any, of lower hydrocarbons.

Alcohol conversion and selectivity of each product were calculated by referring the outlet molar flow to the inlet molar flow of the alcohol, as follows:

$$X_{alcohol} = \frac{(\%mol\ alcohol,\ in - \%mol\ alcohol,\ out)}{(\%mol\ alcohol,\ in)} \times 100$$

$$S_{product} = \frac{\%mol\ i}{(\%mol\ alcohol,\ in - \%mol\ alcohol,\ out)} \times 100$$

3. Results and discussion

3.1. Acidity characterization by FT-IR pyridine adsorption

Polycrystalline CeO_2 possesses different surface Ce to O ratios depending primarily on the type of crystalline planes exposed at the surface. To reduce the surface free energy of Ce, reconstruction occurs by reaction between the ceria surface and molecules from the environment (e.g., water). This leads to the formation of new surface species, such as -OH groups (usually referred to as Brønsted acid sites). The oxygen vacancy is created on CeO_2 by removal of adsorbed water by thermal treatment in the presence of either air or H_2. The unsaturated metal site acts as a Lewis acid center.

IR spectroscopy determines both the nature and strength of catalyst acidity by adsorbing pyridine as a probe molecule. Typically, pyridine adsorbs on Brønsted (Py-B) and Lewis (Py-L) acid sites of CeO_2-MeO_x as shown in **Scheme 1**. The Ce and other metals exposed to surfaces act as Lewis acid (Py-L) sites, and those hydroxyl groups associated with Ce or metals are Brønsted acid (Py-B) sites. Apart from this, pyridine can also adsorb onto oxygen vacancies referred to as redox sites. There is uncertainty in distinguishing the structural differences between the Lewis acid site and oxygen vacancy [42]. In this study, additional complications arise due to the presence of metal other than Ce that might contribute to Brønsted and Lewis acidity as well. Hence, no attempt has been made to differentiate among Lewis acid sites. **Fig. 1** shows the FT-IR spectra of pyridine adsorption on CeO_2 and CeO_2-MeO_x catalysts after pretreatment in H_2 at 500℃. The IR bands at 1550-1540 cm^{-1} correspond to Brønsted acidity, and 1460-1440 cm^{-1} bands are attributed to Lewis acid sites, as shown in **Table 1**.

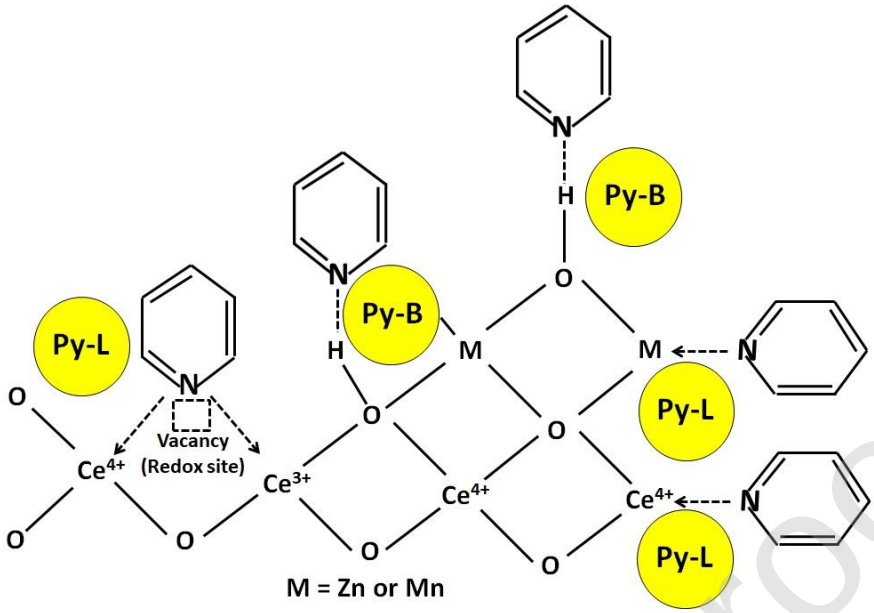

Scheme 1. Adsorption of pyridine on different sites of H_2-treated CeO_2-MeO_x

The H_2-pretreated CeO_2 shows bands at 1545, 1490, and 1445 cm^{-1}. The amount of Brønsted (B) acidity in CeO_2 was 35 μmol/g, and Lewis (L) acidity was 240 μmol/g, as shown in **Scheme 2a**. The oxygen vacant redox sites were generated upon reducing CeO_2 to high temperatures. The addition of 10 wt.% MnO_x increases Brønsted acidity of CeO_2 from 35 to 50 μmol/g, and on the other hand, Lewis acidity dropped from 240 to 143 μmol/g. As MnO_x interacts, it probably consumed a small number of hydroxyl groups on CeO_2, but the acidity data shows the opposite, which indicates that additional B sites must come from MnO_x. The decreasing L sites with MnO_x addition can be explained based on the formation of fewer coordinatively unsaturated Ce metal sites on CeO_2 during reduction. Both B and L sites increase with the addition of ZnO on CeO_2. However, this increase becomes very pronounced for B rather than L with CeO_2-ZnO. The spectra show two types of Lewis acid sites with bands at 1445 and 1455 cm^{-1}. The higher wave number at 1455 cm^{-1} corresponds to pyridine adsorbed on L sites of Zn^{2+} [43]. This suggests that

the addition of ZnO generates new B and L sites in addition to sites that belong to CeO_2. These new B and L sites should be associated with ZnO.

On the other hand, alkaline earth metals (Mg, Ca) and alkali metal (Na) additions tend to decrease both B and L sites. This could be due to the exchange of the acidic proton of CeO_2 with metal cations such as Na^+, Ca^{++}, and Mg^{++}, or due to their oxide phases being well-dispersed on the surface of ceria. However, the former explains only a decrease in B sites, but the latter could explain the depletion of L sites as alkali metal ions show significantly lower acidity than ceria. Additionally, alkali and alkali earth metals could reduce L sites by assisting CO_2 to interact more strongly with CeO_2, preventing oxygen vacancy formation (**Scheme 2a**). Zaki et al. [44] found that Na poisoned the Lewis acid sites on CeO_2 but did not offer any explanation. It is believed that active sites for acid/base catalysis on CeO_2 were generated upon removal of CO_2 and/or H_2O with high-temperature treatments [45]. If this is the case, Na could hamper CO_2 dissociation, as explained earlier in this discussion, leading to fewer oxygen vacancies accompanied by diminished acidity compared to undoped CeO_2. As with CeO_2-MnO_x and CeO_2-ZnO, alkali earth metals (Mg and Ca) also generated much stronger L sites, which displayed a band at 1450-1455 cm^{-1} attributable to the associated metal cations [46,47].

Unlike H_2-pretreatment, air pretreated CeO_2 showed no Brønsted acidity (**Fig. 2**). The air pretreated samples exhibited half of the Lewis sites (117 μmol/g) compared to H_2-pretreated ceria (240 μmol/g). On oxidized CeO_2, Lewis acidity arises due to exposed Ce^{4+} sites with different degrees of coordinative unsaturation as shown in **Scheme 2b**. Among the air-pretreated samples, CeO_2-MnO_x has the maximum number of B sites (250 μmol/g), followed by CeO_2-ZnO (105 μmol/g). The CeO_2 modified by Mg and Ca show traces of B sites while CeO_2-Na_2O displayed

no B sites. The band positions corresponding to B and L sites did not vary appreciably between H_2-pretreated and air-pretreated samples.

In comparison to acid-base properties, the redox function of ceria has been well studied. In the present work, an analysis of FT-IR pyridine adsorption on CeO_2 and CeO_2-MeO_x catalysts after different pretreatment conditions infers that new B and L sites created by the addition of MnO_x or ZnO are due to a charge imbalance between the added metal cation and ceria. Remember ZnO or MnO_x alone can contribute to total acidity. In contrast, both B and L acidity of CeO_2 were found to decrease with the addition of Mg, Ca or Na.

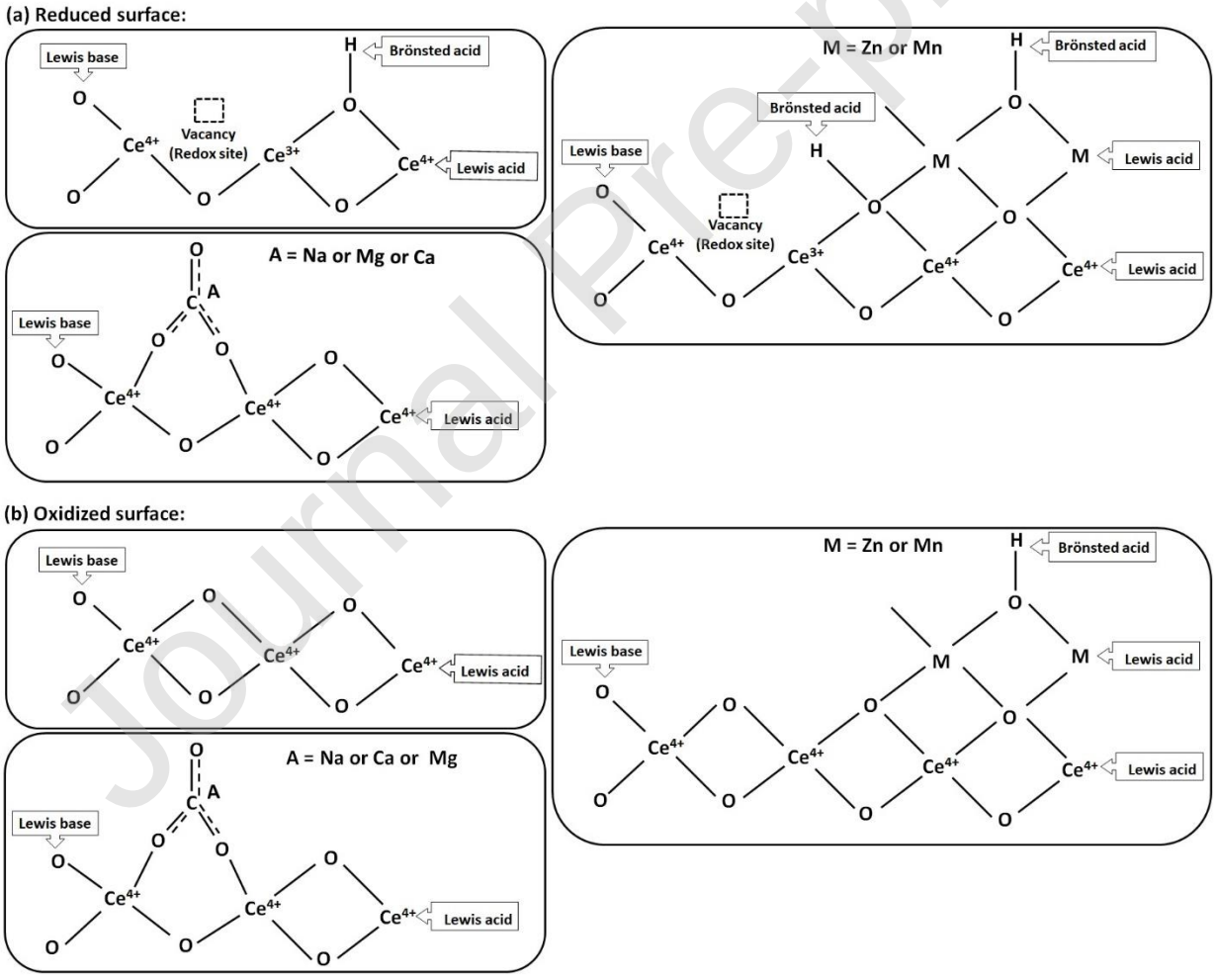

Scheme 2. Proposed structures of acidic and basic sites of (a) H_2-pretreated and (b) oxidized surfaces of CeO_2 and CeO_2-MeO_x catalysts.

3.2 X-ray Absorption Fine Structure Analysis: In-situ H_2-Temperature Programmed Reduction

The XANES technique was employed to monitor changes in the oxidation state of cerium oxide during H_2 treatment at different temperatures. The experimental details of H_2-TPR XANES are provided in Section 2.2. XANES spectra of reference compounds for Ce^{4+} (CeO_2) and Ce^{3+} (cerium carbonate) were published by our group earlier, and we used those spectra for qualitative and quantitative purposes [48]. In general, Ce^{4+} compounds show a white line having two peaks corresponding to $2p_{3/2} \rightarrow (4f^1\underline{L})5d^*$ and $2p_{3/2} \rightarrow (4f^0)5d^*$ transitions. However, Ce^{3+} compounds have a strong absorption edge due to a $2p_{3/2} \rightarrow (4f^1)5d^*$ electronic transition (d^* denotes an excited electron in the d orbital). **Fig. 3** shows a typical XANES spectrum of CeO_2 and CeO_2-MeO_x catalysts. Before reduction, CeO_2 is in a 4+ oxidation state, and the reduction takes place in two stages. The first dip in XANES between 300-500 ℃ is for surface shell reduction of CeO_2 from Ce^{4+} to Ce^{3+} and may be associated with O-vacancy generation and Type-II bridging OH group formation. The second dip at high temperature (>700 ℃) was attributed to the bulk reduction of CeO_2 to Ce_2O_3. Differences in reduction patterns are noticed between samples, especially in the higher temperature region, indicating that the addition of metal oxides influences ceria reduction.

EXAFS analysis reveal the structural characteristics such as the cerium coordination number and the bond length of Ce – O. **Fig. 4** shows the EXAFS spectrum of CeO_2 and CeO_2-MeO_x catalysts. The quantitative EXAFS data are shown in **Table 2** for various samples before and after H_2 treatment. The Ce – O bond length in CeO_2 is 2.341 Å; this distance decreased to 2.338 Å for CeO_2 after high-temperature H_2 treatment, indicating a contraction when ceria loses O, such that the remaining O atoms are held more tightly. This explanation is supported by the

literature [49]. The Ce – O bond length in CeO_2-ZnO and CeO_2-MgO show similar trends as CeO_2 but CeO_2-MnO, CeO_2-CaO, and CeO_2-Na_2O all show either the same Ce – O bond length or even an increase after H_2 treatment. The reason for such an observation is not apparent. As expected, the Ce coordination number (N) for CeO_2 decreased from 4.74 to 2.94 after the high-temperature H_2 treatment due to the loss of surface O. The percentage decrease of N_{Ce-O} from oxidized to reduced for different catalysts follows in the order, CeO_2-Na_2O < CeO_2-MgO < CeO_2-CaO < CeO_2 < CeO_2-ZnO < CeO_2-MnO_x. The results of the fittings suggest that Mn and Zn containing CeO_2 lose relatively more oxygen than CeO_2 or Ca-, Mg-, and Na-modified CeO_2 during hydrogen reduction.

The degree of ceria reduction, as shown in **Fig. 5**, was quantified using the XANES spectra of different treated catalysts. The initial Ce^{4+} concentration is assumed to be 100%; however, the Ce^{4+} content falls below 90% at 500 ℃ and further diminishes to 50% at 700 ℃. In contrast, the Ce^{3+} concentration increases with temperature. CeO_2 and CeO_2-Na_2O catalysts show a very similar reduction profile, while metal oxide addition inhibited ceria reduction for CeO_2-MnO_x, CeO_2-ZnO, CeO_2-MgO, and CeO_2-CaO. Surface shell reduction of ceria began at 200 ℃, and this point shifted slightly to higher temperature for all metal oxide modified CeO_2 catalysts as directed by the arrow shown in **Fig. 5**. It indicates that the added metal oxides on ceria somehow stabilize O on the surface by forming solid solutions [50]. However, reports on Mn or Zn additions have found enhanced ceria reduction due to the formation of more labile oxygen with mixed solid solutions compared to undoped CeO_2. Given the fact that the magnitude of the difference in the oxidation state of Ce is trivial between samples up to a pretreatment temperature of 500 ℃, it is difficult to make any definitive conclusion. Nevertheless, H_2-TPR XANES/EXAFS provided

quantitative details on the cerium oxidation state, as well as oxygen vacancy formation, before and after the treatment in H_2.

3.3 Dehydration of 1,5-pentanediol and cyclohexanol

Table 3 shows conversion and selectivity for the dehydration of 1,5-pentanediol on CeO_2 and metal-oxide modified-CeO_2 catalysts after different pretreatment conditions. The products are 1-propanol, tetrahydropyran, tetrahydropyran-2-one, 4-penten-1-ol, 1-pentanol, cyclopentanol, cyclopentanone, 3,4-dihydropyran, 2-methylcyclopentanone, cyclohexylmethanol, 4-pentenyl propionate, 4-pentenyl pentanoate, cyclohexyl cyclohexanecarboxylate, 2,2-dimethyl 3-octanol. There are also esters of high molecular weight formed whose mechanism of formation remains uncertain. Due to this reason, a complete material balance cannot be achieved. The conversion of 1,5-PDO with H_2-treated CeO_2-MnO_x and CeO_2-ZnO samples is relatively higher than CeO_2. On the other hand, basic metals such as Mg, Ca, and Na tended to decrease the diol conversion. However, catalytic activity of air-pretreated catalysts followed the order: CeO_2 > CeO_2-MnO_x > CeO_2-MgO > CeO_2-ZnO > CeO_2-CaO > CeO_2-Na_2O. Irrespective of catalyst and treatment conditions, five-membered cyclic products such as cyclopentanol and cyclopentanone were formed to a significant extent (20-35%) other than THP and THP-2-one. The selectivity to linear alcohols (4-penten-1-ol+1-pentanol) on H_2-treated catalysts were 34.4%, 30.6%, 28.1%, 41.5%, 30.8% and 64.9% for CeO_2, CeO_2-MnO_x, CeO_2-ZnO, CeO_2-MgO, CeO_2-CaO and CeO_2-Na_2O, respectively. Similarly, linear alcohol selectivity for air-pretreated catalysts varied between 25-46%. The product labeled as "Others" contributed about 5-22% to total products formed. The data showed that pretreatment conditions do affect the dehydration capability of CeO_2 and modified-CeO_2 catalysts. **Fig. 6** shows a linear relationship between the selectivity of different products and the conversion of 1,5-PDO. H_2-pretreated samples show relatively higher selectivity

to linear alcohols (4-penten-1-ol and 1-pentanol) than air-pretreated catalysts at a similar conversion level. The results in **Fig. 6** indicated that at higher conversions, cyclization is more preferred than linear products. The air-pretreated samples show a steeper slope (negative for linear alcohols and positive in the case of cyclized products) compared to H_2-pretreated samples, indicating H_2-treatment is an added advantage over air pretreatment to achieve a higher selectivity to linear alcohols.

The dehydration capability of the catalysts was investigated using cyclohexanol dehydration as a probe reaction. Cyclohexanol can undergo dehydration to cyclohexene over Brønsted acid sites; on the other hand, basic sites - in this case, lattice oxygen ions - catalyze dehydrogenation that lead to cyclohexanone [51]. Hence, the ratio of the products sheds light on the acidic and basic sites present on these catalysts. The reaction data shown in **Table 4** were obtained using H_2 and air-pretreated samples. In general, CeO_2-based catalysts are not as selective as other rare-earth oxides for the dehydration reaction [27]. In the current study, the ratio of cyclohexene/cyclohexanone was below 0.5, which indicates that dehydrogenation is a preferred reaction either on air-pretreated or H_2-pretreated samples. The percentage cyclohexanol conversion on CeO_2-MnO_x and CeO_2-ZnO was higher than CeO_2 alone under both pretreatment conditions, while CeO_2-MgO, CeO_2-CaO, and CeO_2-Na_2O exhibited lower activity. These results coincide with those from the dehydration of 1,5-pentanediol reaction.

On the other hand, CeO_2 and CeO_2-MgO catalysts produce dehydration products equivalently (~30%), and far better than any samples tested for this study. The H_2-pretreated catalysts all show much less dehydration selectivity (<13%) compared to air-pretreated samples. Overall, MnO_x and ZnO accelerate cyclohexanol conversion, and this is probably linked to the production of additional acid sites. The results also show that basic sites associated with lattice

oxygen are responsible for higher dehydrogenation selectivity ($C_6^=$/C_6-one) on H_2-pretreated samples.

3.4 Relationship between acidity and dehydration activity and selectivity

It is generally accepted that the dehydration on heterogeneous catalysts requires both acidic and basic sites [4]. In this respect, 1,5-pentanediol conversion, as shown in **Fig. 7**, increases with increasing Brønsted acidity, irrespective of pretreatment conditions and the nature of the catalyst. Similarly, H_2-pretreated catalysts display a linear relationship between conversion of 1,5-PDO and total acidity, indicating that both Brønsted and Lewis acidity contribute to the transformation of 1,5-PDO. However, air-pretreated samples show scattered points for the plot of Lewis acidity versus dehydration activity. The added metal oxide might have interfered with the acidic function, as well as the adsorption and desorption characteristics of 1,5-PDO on CeO_2, that ultimately determine catalyst activity. The air-pretreated catalysts show twice the amount of acid sites as compared to H_2-pretreated catalysts; indeed, acidity did not translate entirely to catalyst activity. For example, CeO_2-MnO_x and CeO_2-ZnO after air-pretreatment displayed Lewis acidity > 300 μmol/g, which is nearly twice that of H_2-treated catalysts. Despite its lower acidity, H_2-pretreated CeO_2-MnO_x and CeO_2-ZnO samples showed higher diol conversion compared to corresponding air-pretreated samples. One possible reason is that the structure and location of Lewis acid sites on the oxidized catalyst may be different from the H_2-treated sample. Another reason could be the lack of associated basic sites near Lewis acid sites on the oxidized surface, which will limit H abstraction from the β-carbon required to form dehydration products. In both cases, acidity alone cannot contribute to the conversion of 1,5-PDO. The cyclohexanol conversion on both air- and H_2-pretreated CeO_2 and CeO_2-MeO_x catalysts show a linear correlation with Brønsted acid sites.

A similar relationship can be seen between Lewis acidity and cyclohexanol conversion (**Fig. 8**) which implies that both B and L sites contribute to cyclohexanol conversion.

The ratio of linear-to-cyclized products obtained on both H_2- and air-pretreated samples for dehydration of 1,5-PDO decreases with increasing the number of B sites. However, the ratio achieved a maximum Lewis acidity of 200 μmol/g and then dropped with further increases in the number of L sites (**Fig. 9**). At the same time, air-pretreated samples showed a decreasing trend over the entire range of Lewis acidity. Unlike 1,5-PDO, which involves a variety of reactions, cyclohexanol undergoes either dehydration or dehydrogenation on ceria. **Fig. 10** shows the relationship between acidity and dehydration/dehydrogenation products ratio. Apart from CeO_2 and CeO_2-MgO, the dehydration/dehydrogenation ratio remains below 0.15 for all other samples, indicating that they are highly selective towards dehydrogenation. The dehydration/dehydrogenation ratio decreases with increasing B and L sites.

H_2-reduced ceria exhibits oxygen vacancies (i.e., redox sites) along with acid-base sites. Several groups reported that dehydration that leads to the production of olefins from alcohol is considered an acid-catalyzed reaction, while dehydrogenation is considered basic catalysis. Rare-earth oxides like CeO_2 contain oxygen vacancies or defect sites, providing an additional active center for dehydration. The vacancy site on ceria is viewed as the primary reaction site for diol [27]. Terminal diols like 1,5-pentenediol readily undergo cyclization over ceria producing tetrahydropyran and cyclopentanol. In this study, we propose mechanisms for the formation of different products from 1,5-pentanediol dehydration. Several factors, including geometry, the combination of acid-base and redox sites, and their location, determine the mode of adsorption of 1,5-PDO. The sites available next to those oxygen vacancies (i.e., Lewis base or Brønsted acid) probably guiding the reaction pathway (i.e., via β-H abstraction if Lewis base sites are involved or

via unimolecular H^+ addition by Brønsted acid sites, as shown in **Scheme 3a, 3b**). Alternatively, the adsorbed diol might undergo cyclization to tetrahydropyran as well (**Scheme 3c**).

The air-pretreated samples, particularly CeO_2-MnO_x and CeO_2-ZnO, contain relatively more acid sites compared to H_2-pretreated samples, but alcohol conversion on air-pretreated catalysts was rather low. It is believed to be due to differences in the oxygen vacancy densities between air pretreated and H_2-pretreated samples, because the former is less active than the latter. Thus, we conclude that oxygen vacancies (redox sites) coupled with basic or acidic sites seem to be responsible for the activity of dehydration of 1,5-PDO on CeO_2-based catalysts. The product selectivity to unsaturated or saturated linear alcohols decreases with increasing B and L sites, independent of the pretreatment conditions. CeO_2-Na_2O and CeO_2-MgO show higher unsaturated alcohol selectivity than any other catalysts tested, probably due to complementary basic sites provided by those metal oxides (i.e., without adding significantly more acidity to the catalysts).

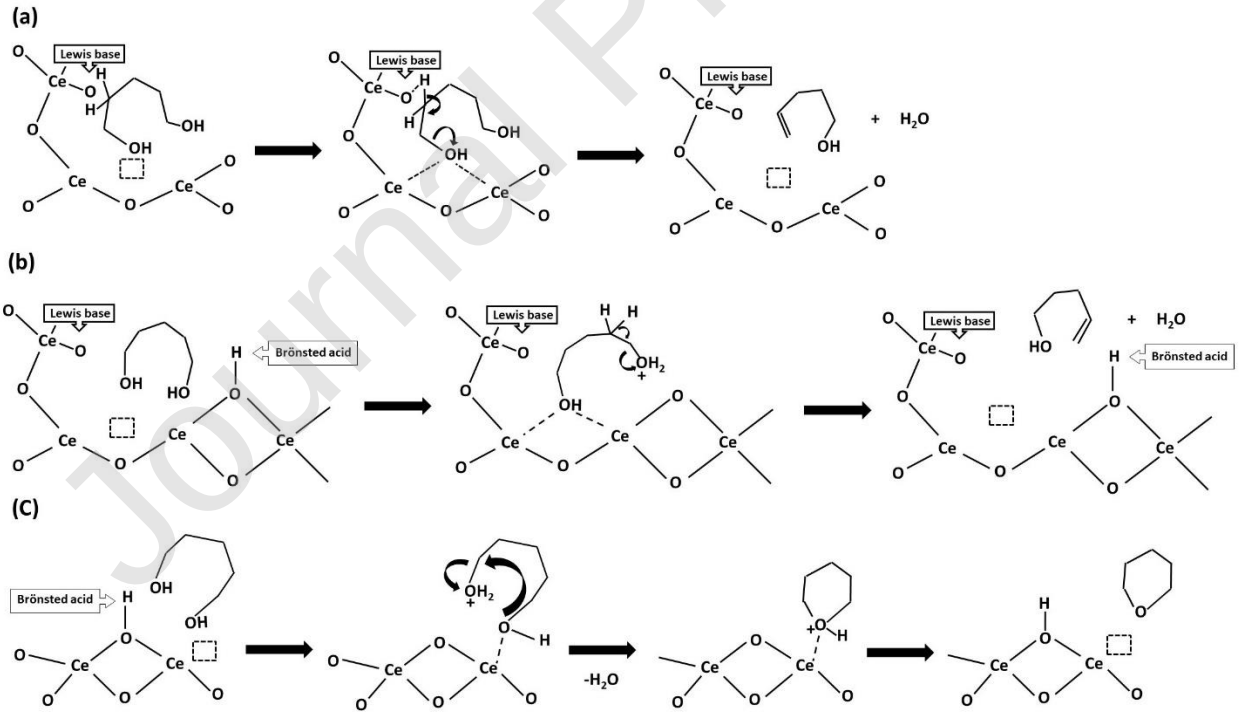

Scheme 3. A plausible reaction mechanism, (a) Lewis base-assisted; (b) Brønsted acid-assisted; and (c) Brønsted acid-assisted ring closure, for the formation of different products from dehydration of 1,5-PDO on reduced CeO_2 catalysts.

4. Conclusions

The dehydration of 1,5-pentanediol was investigated on CeO_2 and MeO_x-modified CeO_2 catalysts after air and H_2-pretreatments. The acidity measured by pyridine adsorption on oxidized and reduced catalysts reveals that MnO_x and ZnO increase the Brønsted and Lewis acidity of CeO_2. From a H_2-TPR XANES/EXAFS study, the degree of ceria reduction was observed to be influenced by the presence of the added metal oxide. The conversion of 1,5-PDO or cyclohexanol increases with the addition of MnO_x and ZnO on ceria while MgO, CaO, and Na_2O suppressed the overall alcohol conversion, but improved the selectivity to linear alcohols. The catalyst activity increases linearly with increasing Brønsted and Lewis acidity, indicating that both sites take part in the reaction. In contrast, the linear-to-cyclized product ratio in the case of 1,5-PDO, or dehydration-to-dehydrogenation product ratio in the case of cyclohexanol, decreased with increasing Brønsted acidity on H_2 and air-pretreated catalysts. There must be an optimum density of Lewis acid sites (160-200 mmol/g) required for CeO_2-based catalysts to achieve higher dehydration selectivity. The oxygen vacancies are primary adsorption sites on CeO_2 for 1,5-PDO, and further reaction of dehydration, dehydrocylization or dehydrogenation depends mainly on the mode of interaction of alcohol and acid-base sites located within close vicinity to oxygen vacancies.

CRediT author statement

M.K. Gnanamani: Conceptualization, Methodology, Investigation, Writing **R. Garcia:** Formal analysis, Investigation **G. Jacobs:** Formal analysis, Data Curation, Validation, Review & Editing

K.Góra-Marek: Formal analysis, Investigation, Data curation **D.C. Cronauer:** Investigation, Resources **A.J. Kropf:** Formal analysis, Data Curation, Investigation, Resources **C.L. Marshall:** Investigation, Resources

Acknowledgment

The work carried out at the CAER was supported in part by funding from the Commonwealth of Kentucky. Research conducted at UTSA was supported by UTSA, the State of Texas, and the STARs program. Richard Garcia would like to acknowledge funding from a UTSA College of Engineering Scholarship. His work was also supported by the USDA National Institute of Food and Agriculture, Interdisciplinary Hands-on Research Traineeship and Extension Experiential Learning in Bioenergy/Natural Resources/Economics/Rural project, U-GREAT (Undergraduate Research, Education and Training) program (2016-67032-24984). Argonne's research was supported in part by the U.S. Department of Energy (DOE), Office of Fossil Energy, National Energy Technology Laboratory (NETL). Advanced Photon Source was supported by the U.S. Department of Energy, Office of Science, Office of Basic Energy Sciences, under Contract No. DE-AC02-06CH11357. MRCAT operations are supported by the Department of Energy and the MRCAT member institutions.

References

1. B.H. Davis, "Alcohol conversion selectivity as a measure of the base strength of metal oxide catalysts" Stud. Surf. Sci. Catal. 21 (1985) 309-318.

2. D.J. Collins, J.C. Watters, B.H. Davis, “Catalytic conversion of alcohols. XIII: Alkane selectivity with TiO2 catalysts” Ind. Eng. Chem. Prod. Res. Dev., 18 (1979) 202-205.

3. B. Shi and B.H. Davis, “Alcohol dehydration: Mechanism of ether formation using an alumina catalyst” J. Catal. 157 (1995) 359-367.

4. H. Knözinger, “Dehydration of alcohols on aluminum oxide” Angew. Chem. Int. Ed. 7 (1968) 791-805.

5. M.K. Gnanamani, G. Jacobs, W.D. Shafer, B.H. Davis, “Dehydration of 2-octanol over Ca-doped CeO2 catalysts” ChemCatChem 9 (2017) 492-498.

6. B.H. Davis and W.S. Brey Jr. “Dehydration and dehydrogenation of 2-octanol by thorium oxide” J. Catal. 25 (1972) 81-92.

7. S. Chokkaram and B.H. Davis, “Dehydration of 2-octanol over zirconia catalysts: Influence of crystal structure, sulfate addition and pretreatment” J. Mol. Catal. A: Chem. 118 (1997) 89-99.

8. B.H. Davis, “Influence of pretreatment of alumina on the dehydrogenation:dehydration selectivity for 2-octanol” J. Catal. 26 (1972) 348-251.

9. B.H. Davis and P. Ganesan, “Catalytic conversion of alcohols. 11. Influence of preparation and pretreatment on the selectivity of zirconia” Ind. Eng. Chem. Prod. Res. Dev. 18 (1979) 191-198.

10. P. Berteau, B. Delmon, J.-L. Dallons, A. Van Gysel, “Acid-base properties of silica-aluminas: use of 1-butanol dehydration as a test reaction” Appl. Catal. A: Gen. 70 (1991) 307-323.

11. D. Devaiah, L.H. Reddy, S.-Eon Park, B.M. Reddy, “Ceria-Zirconia mixed oxides: Synthetic methods and applications” Catal. Rev. Sci. Eng. 60 (2018) 177-277.

12. Q. Zhuang, J.M. Miller, “ZrO2/SiO2 mixed oxides as catalysts for alcohol dehydration” Appl. Catal. A: Gen. 209 (2001) L1-L6.

13. V.N. Viter, P.G. Nagornyi, “Synthesis and study of solid acid materials SnO2/B2O3” Russ. J. Appl. Chem. 82 (2009) 209-212.

14. M.P. Rosynek, “Catalytic properties of Rare Earth Oxides” Catal. Rev. Sci. Eng. 16 (1977) 111-154.

15. A. Trovarelli, “Catalytic properties of Ceria and CeO2-containing materials” Catal. Rev. Sci. Eng. 38 (1996) 439-520.

16. D.R. Mullins, “The surface chemistry of Cerium Oxide” Surf. Sci. Rep. 70 (2015) 42-85.

17. G. Adachi, N. Imanaka, “The binary Rare Earth Oxides” Chem. Rev. 98 (1998) 1479-1514.

18. T. Montini, M. Melchionna, M. Monai, P. Fornasiero, “Fundamentals and catalytic applications of CeO2-based materials” Chem. Rev. 116 (2016) 5987-6041.

19. F. Esch, S. Fabris, L. Zhou, T. Montini, C. Africh, P. Fornasiero, G. Comelli, R. Rosei, “Electron localization determines defect formation on ceria substrates” Science 309 (2005) 752-755.

20. A. Badri, C. Binet, J.-C. Lavalley, “An FTIR study of ceria hydroxyl groups during a redox process with H2” J. Chem. Soc., Faraday Trans., 92 (1996) 4669-4673.

21. D. Mullins, S.D. Senanayake, T.-L. Chen, “Adsorption and reaction of C1-C3 alcohols over CeOx (111) thin films” J. Phys. Chem. C 114 (2010) 17112-17119.

22. K. Mudiyanselage, I. Al-Shankiti, A. Foulis, J. Llorca, H. Idriss, “Reactions of ethanol over CeO2 and Ru/CeO2 catalysts” Appl. Catal. B: Environ. 197 (2016) 198-205.

23. G. Jacobs, R.A. Keogh, B.H. Davis, “Steam reforming of ethanol over Pt/ceria with co-fed Hydrogen” J. Catal. 245 (2007) 326-337.

24. N. Ohtake, Y. Yamane, K. Nakagawa, M. Katoh, S. Sugiyama, "Hydrothermally synthesized ceria with high specific area for catalytic conversion of ethanol to ethylene" J. Chem. Eng. Jpn. 49 (2016) 197-203.

25. M. Zaki and N. Sheppard, "An Infrared spectroscopic study of the adsorption and mechanism of surface reactions of 2-propanol on Ceria" J. Catal. 80 (1983) 114-122.

26. S. Sato, R. Takahashi, T. Sodesawa, N. Honda, "Dehydration of diols catalyzed by CeO2" J. Mol. Catal. A: Chem. 221 (2004) 177-183.

27. S. Sato, F. Sato, H. Gotoh, Y. Yamada, "Selective dehydration of alkanediols into unsaturated alcohols over Rare Earth Oxide catalysts" ACS Catal. 3 (2013) 721-734.

28. S. Sato, R. Takahashi, M. Kobune, H. Inoue, Y. Izawa, "Dehydration of 1,4-butanediol over rare earth oxides" Appl. Catal. A: Gen. 356 (2009) 64-71.

29. M. Segawa, S. Sato, M. Kobune, T. Sodesawa, T. Kojima, S. Nishiyama, N. Ishizawa, "Vapor-phase catalytic reactions of alcohols over bixbyite indium oxide" J. Mol. Catal. A: Chem. 310 (2009) 166-173.

30. K. Abe, Y. Ohishi, T. Okada, Y. Yamada, S. Sato, "Vapor-phase catalytic dehydration of terminal diols" Catal. Today 164 (2011) 419-424.

31. H. Gotoh, Y. Yamada, S. Sato, "Dehydration of 1,3-butanediol over rare earth oxides" Appl. Catal. A: Gen. 377 (2010) 92-98.

32. M.K. Gnanamani, G. Jacobs, M. Martinelli, W.D. Shafer, S.D. Hopps, G.A. Thomas, B.H. Davis, "Dehydration of 1,5-Pentanediol over Na-doped CeO2 catalysts" ChemCatChem 10 (2018) 1148-1154.

33. M.K. Gnanamani, M. Martinelli, S. Badoga, S.D. Hopps, B.H. Davis, "Dehydration of 1,5-Pentanediol over CeO2-MeOx catalysts" ChemCatChem 10 (2018) 4629-4635.

34. K.A. Tarach, K.G.-Marek, J.M.-Triguero, I.M.-Cabrera, "Acidity and accessibility of desilicated SZM-5 zeolites in terms of their effectiveness as catalysts in acid-catalyzed cracking processes" Catal. Sci. Technol. 7 (2017) 858-873.

35. K.G.-Marek, M. Derewinski, J. Datka, P. Sarv, "IR and NMR studies of mesoporous alumina and related aluminosilicates" Catal. Today 101 (2005) 131-138.

36. M. Jacoby, X-ray absorption spectroscopy. Chem Eng News 79 (2001) 33-8.

37. T. Ressler: a Program for X-ray Absorption Spectroscopy Data Analysis under MS-Windows. J Synchrotron Rad 5 (1998) 118-122.

38. L.Z. Linganiso, G. Jacobs, K.G. Azzam, U.M. Graham, B.H. Davis, D.C. Cronauer, A.J. Kropf, C.L. Marshall, "Low-temperature water-gas shift: Strategy to lower Pt loading by doping Ceria with Ca2+ improves formate mobility/WGS rate by increasing surface O-mobility" Appl. Catal. A: Gen. 394 (2011) 105–116.

39. B. Ravel, ATOMS: crystallography for the X-ray absorption spectroscopist, J Synchrotron Rad 8 (2001) 314-6.

40. M. Newville, B. Ravel, D. Haskel, J.J. Rehr, A.A. Stern, Y. Yacoby. Analysis of multiple-scattering XAFS data using theoretical standards. Physica B: Condensed Matter 208-209 (1995) 154-6.

41. W.A. Dietz, "Response factors for gas chromatographic analyses" J. Gas Chromatogr. 5 (1967) 68-71.

42. X. Ren, Z. Zhang, Y. Wang, J. Lu, J. An, J. Zhang, M. Wang, X. Wang, Y. Luo, "Capping experiments reveal multiple surface active sites in CeO2 and their cooperative catalysis" RSC Adv., 9 (2019) 15229-15237.

43. O.V. Larina, P.I. Kyriienko, D.Y. Balakin, M. Vorokhta, I. Khalakhan, Y.M. Nychiporuk, V. Matolin, S.O. Soloviev, S.M. Orlyk, "Effect of ZnO on acid-base properties and catalytic performances of ZnO/ZrO2-SiO2 catalysts in 1,3-butadiene production from ethanol-water mixture" Catal. Sci. Technol., 9 (2019) 3964-3978.

44. M.I. Zaki, G.A.M. Hussein, S.A.A. Mansour, H.A.El.-Ammawy "Adsorption and surface reactions of pyridine on pure and doped ceria catalysts as studied by infrared spectroscopy" J. Mol. Catal. 51 (1989) 209-220.

45. T. Yamaguchi, N. Ikeda, H. Hattori, K. Tanabe, "Surface and catalytic properties of cerium oxide" J. Catal. 67 (1981) 324-330.

46. J.A. Lercher, "Acid-base properties of Al2O3/MgO oxides, II. Infrared study of adsorption of pyridine" React. Kinet. Catal. Lett. 20 (1982) 409-413.

47. H.M.-Yuan, L. Zhonghui, M. Enze, "Acidic and hydrocarbon catalytic properties of pillared clay" Catal. Today 2 (1988) 321-338.

48. L.Z. Linganiso, V.R.R. Pendyala, G. Jacobs, B.H. Davis, D.C. Cronauer, A.J. Kropf, C.L. Marshall, "Low-Temperature Water-gas shift: Doping Ceria improves reducibility and mobility of O-bound species and catalyst activity" Catal. Lett. 141 (2011) 1723-1731.

49. E. Fonda, D. Andreatta, P.E. Colavita, G. Vlaic, "EXAFS analysis of the L3 edge of Ce in CeO2: effects of multi electron excitations and final-state mixed valance" J. Synchrotron Rad. 6 (1999) 34-42.

50. M. Yang, G. Shen, M. Liu, Y. Chen, Z. Wang, Q. Wang, "Preparation of Ce-Mn composite oxides with enhanced catalytic activity for removal of benzene through oxalate method" Nanomaterials 9 (2019) 197-11.

51. C.P. Bezouhanova, M.A. Al-Zihari, “Cyclohexanol conversion as a test of the acid-base properties of metal oxide catalysts” Catal. Lett. 11 (1991) 245-248.

Table 1 Acidity data for CeO_2 and CeO_2-MeO_x catalysts from IR-pyridine adsorption after different pretreatments

Sample	H_2-pretreated				air-pretreated			
	Brønsted acidity		Lewis acidity		Brønsted acidity		Lewis acidity	
	IR-Py bands	amount (μmol/g)	IR-Py bands	amount (μmol/g)	IR-Py bands	amount (μmol/g)	IR-Py bands	amount (μmol/g)
CeO_2	1545	35	1445	240	-	-	1445	117
CeO_2-MnO_x	1543	50	1446	143	1544	250	1446	335
CeO_2-ZnO	1547	85	1445, 1455	263	1545	105	1444, 1455	490
CeO_2-MgO	1544	15	1445, 1450	195	1546	10	1444, 1451	130
CeO_2-CaO	1545	10	1445, 1451	168	1546	7	1444, 1452	135
CeO_2-Na_2O	-	-	1444	140	-	-	1444	120

Table 2 Results of EXAFS fittings at ambient temperature before and after TPR-EXAFS/XANES in H_2/He. Fitting ranges were $\Delta k = 2.5 – 10$ Å^{-1} and $\Delta R = 1.0 – 2.5$ Å.

Sample Description	N Ce-O	R Ce-O (Å)	e_0 (eV)	σ^2 (Å^2)	r-factor
CeO_2 (before)	4.74 (1.08)	2.341 (0.053)	9.05 (3.12)	0.00702 (0.00570)	0.0028
CeO_2 (after)	2.94 (0.63)	2.338 (0.039)	8.83 (2.30)		
CeO_2-MnO_x (before)	4.34 (0.33)	2.332 (0.018)	8.75 (1.03)	0.00611 (0.00200)	0.0031
CeO_2-MnO_x (after)	2.40 (0.18)	2.333 (0.014)	7.67 (0.85)		
CeO_2-ZnO (before)	4.93 (0.45)	2.337 (0.021)	8.75 (1.15)	0.00737 (0.00245)	0.0042
CeO_2-ZnO (after)	2.82 (0.25)	2.284 (0.018)	5.76 (1.09)		
CeO_2-MgO (before)	4.95 (0.55)	2.355 (0.026)	10.0 (1.54)	0.00750 (0.00294)	0.0028
CeO_2-MgO (after)	3.44 (0.39)	2.281 (0.020)	5.52 (1.30)		
CeO_2-CaO (before)	4.34 (0.39)	2.320 (0.022)	8.22 (1.32)	0.00461 (0.00216)	0.0025
CeO_2-CaO (after)	2.83 (0.23)	2.336 (0.015)	8.60 (0.90)		
CeO_2-Na_2O (before)	3.80 (1.01)	2.333 (0.057)	8.56 (3.36)	0.00696 (0.00675)	0.0034
CeO_2-Na_2O (after)	2.78 (0.70)	2.349 (0.049)	9.92 (2.80)		

* note that S_0^2 was fixed at 0.90 as a first approximation.

Table 3 Dehydration of 1,5-pentanediol on CeO_2 and CeO_2-MeO_x after different pretreatments

Sample	% conversion of 1,5-pentanediol[a]	Product distribution (mol%)							
		Propanol	THP	THP-2-one	4-penten-1-ol	1-pentanol	CyP-ol	CyP-one	others[b]
CeO_2-H_2 pretreated	44.2	0.0	0.0	26.8	18.5	15.9	5.4	21.5	11.9
CeO_2-MnO_x	50.7	3.0	0.0	23.7	17.4	13.2	0.0	30.0	12.7
CeO_2-ZnO	58.4	1.8	0.0	30.8	18.3	9.8	19.3	13.9	6.1
CeO_2-MgO	31.2	2.5	0.0	23.5	24.1	17.4	7.0	18.8	6.7
CeO_2-CaO	18.6	5.3	1.4	29.5	15.2	15.6	6.6	6.3	20.1
CeO_2-Na_2O	10.8	0.0	0.0	0.0	36.1	28.8	0.0	12.6	22.5
CeO_2-air pretreated	42.5	9.8	3.7	25.6	13.0	11.5	7.2	20.4	8.8
CeO_2-MnO_x	40.3	1.9	1.0	35.2	22.1	11.5	4.1	17.8	6.4
CeO_2-ZnO	28.3	2.6	0.0	25.6	20.7	6.9	4.7	23.5	16.0
CeO_2-MgO	31.6	3.9	0.0	17.5	21.4	13.5	6.2	28.6	8.9
CeO_2-CaO	24.1	2.7	2.6	14.9	25.3	18.9	4.7	19.9	11.0
CeO_2-Na_2O	20.1	4.3	2.7	10.6	26.5	19.7	5.0	20.2	11.0

[a]Reaction condition: T= 350 °C, P= 1 atm, LHSV= 0.6 ml/h, carrier gas= H_2 or N_2 (50 sccm), 1.0 g catalyst; [b]others included ethanol, 1-propanol, 3,4-dihydropyran, 2-methyl cyclopentanone, cyclohexylmethanol, 4-pentenyl propionate, 4-pentenyl pentanoate, cyclohexyl cyclohexanecarboxylate, 2,2-dimethyl 3-octanol.

Table 4 Cyclohexanol conversion on CeO_2 and CeO_2-MeO_x after different pretreatments

Sample	air-pretreated[a]				H_2-pretreated[b]			
	% conversion of cyclohexanol[e]	selectivity (%)		$C_6^{=}$/ C_6-one	% conversion of cyclohexanol[e]	selectivity (%)		C_6=/ C_6-one
		$C_6^{=c}$	C_6-one[d]			$C_6^{=c}$	C_6-one[d]	
CeO_2	8.8	32.8	67.2	0.488	25.3	1.7	98.3	0.017
CeO_2-MnOx	14.6	8.7	91.3	0.095	24.4	4.7	95.3	0.049
CeO_2-ZnO	38.5	1.1	98.9	0.011	51.9	1.2	98.8	0.012
CeO_2-MgO	6.9	29.2	70.8	0.412	11.4	9.0	91.0	0.099
CeO_2-CaO	4.4	10.2	89.8	0.114	4.7	12.2	87.8	0.139
CeO_2-Na_2O	4.0	6.3	93.7	0.067	3.9	12.9	87.1	0.148

[a]pretreatment condition: 350 °C, air flow (50 sccm), 2 h; [b]pretreatment condition: 500 °C, H_2 flow (50 sccm), 2 h; [c]cyclohexene; [d]cyclohexanone; [e]reaction condition: 350 °C, LHSV = 3.0 ml/h, carrier gas = H_2 or N_2 (50sccm), 0.5 g catalyst.

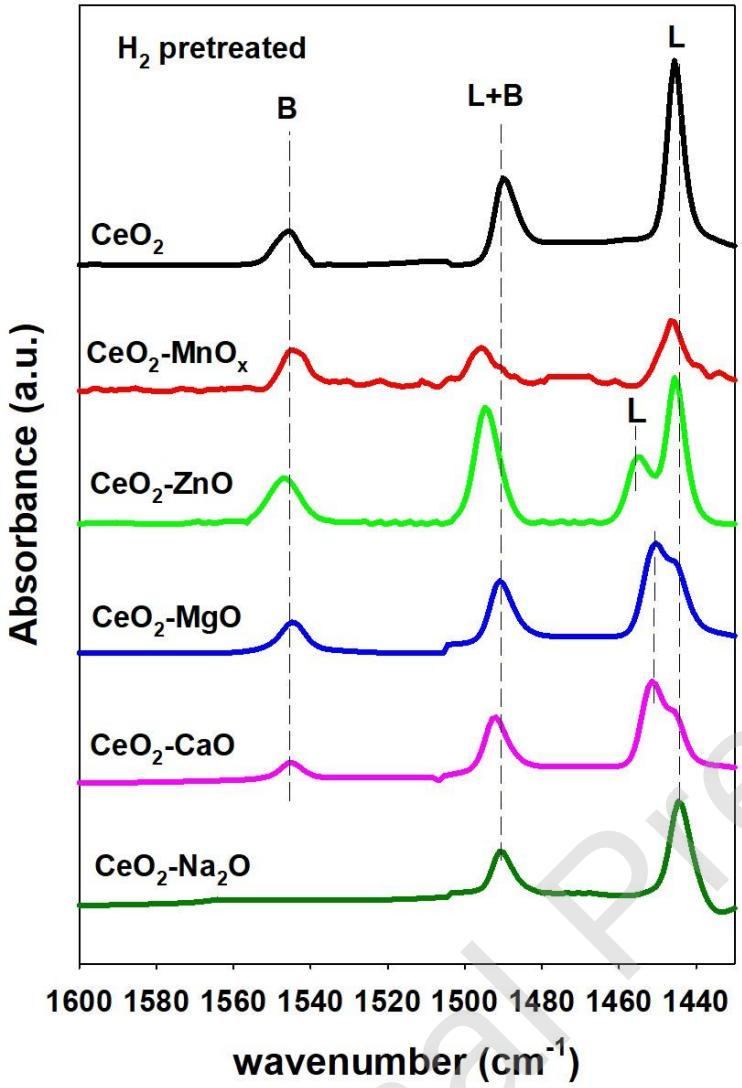

Fig. 1 Infrared spectra of pyridine adsorbed on CeO_2 and CeO_2-MeO_x catalysts after pretreatment in H_2 (500 ℃ for 1 h) following pyridine adsorption and evacuation at 130 ℃ (B-Brønsted acidity, L-Lewis acidity).

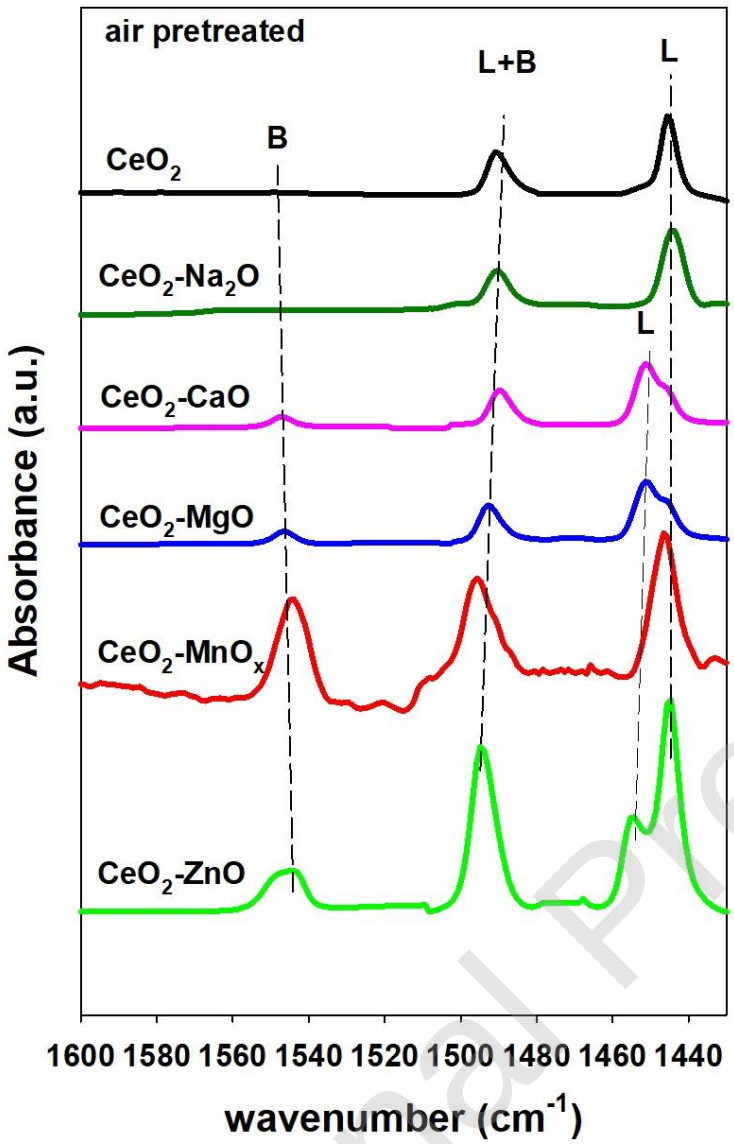

Fig. 2 Infrared spectra of pyridine adsorbed on CeO_2 and CeO_2-MeO_x catalysts after pretreatment in air (350 ℃ for 1 h) following pyridine adsorption and evacuation at 130 ℃ (B-Brønsted acidity, L-Lewis acidity).

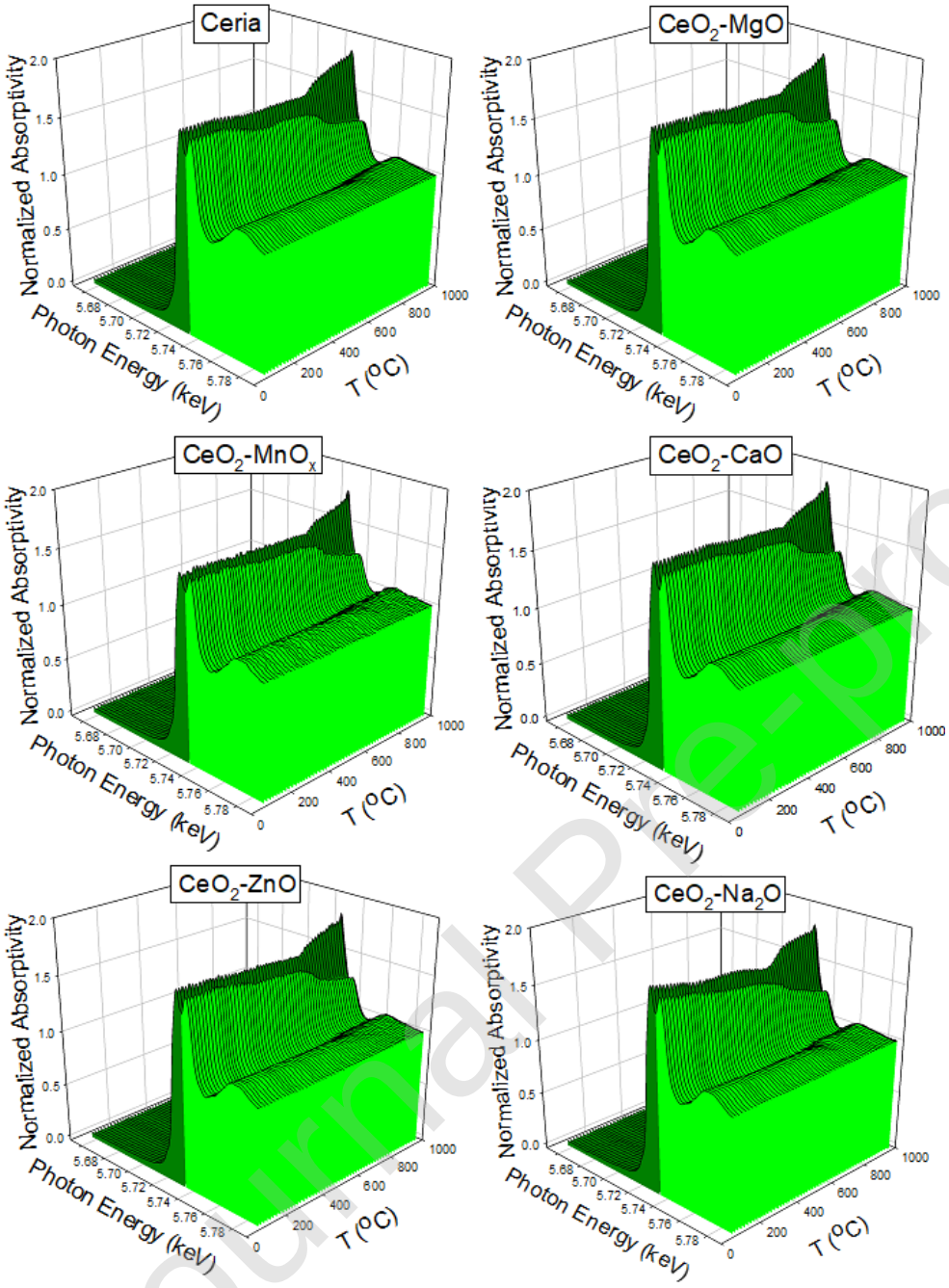

Fig. 3 H_2-TPR-XANES spectra of CeO_2 and CeO_2-MeO_x catalysts

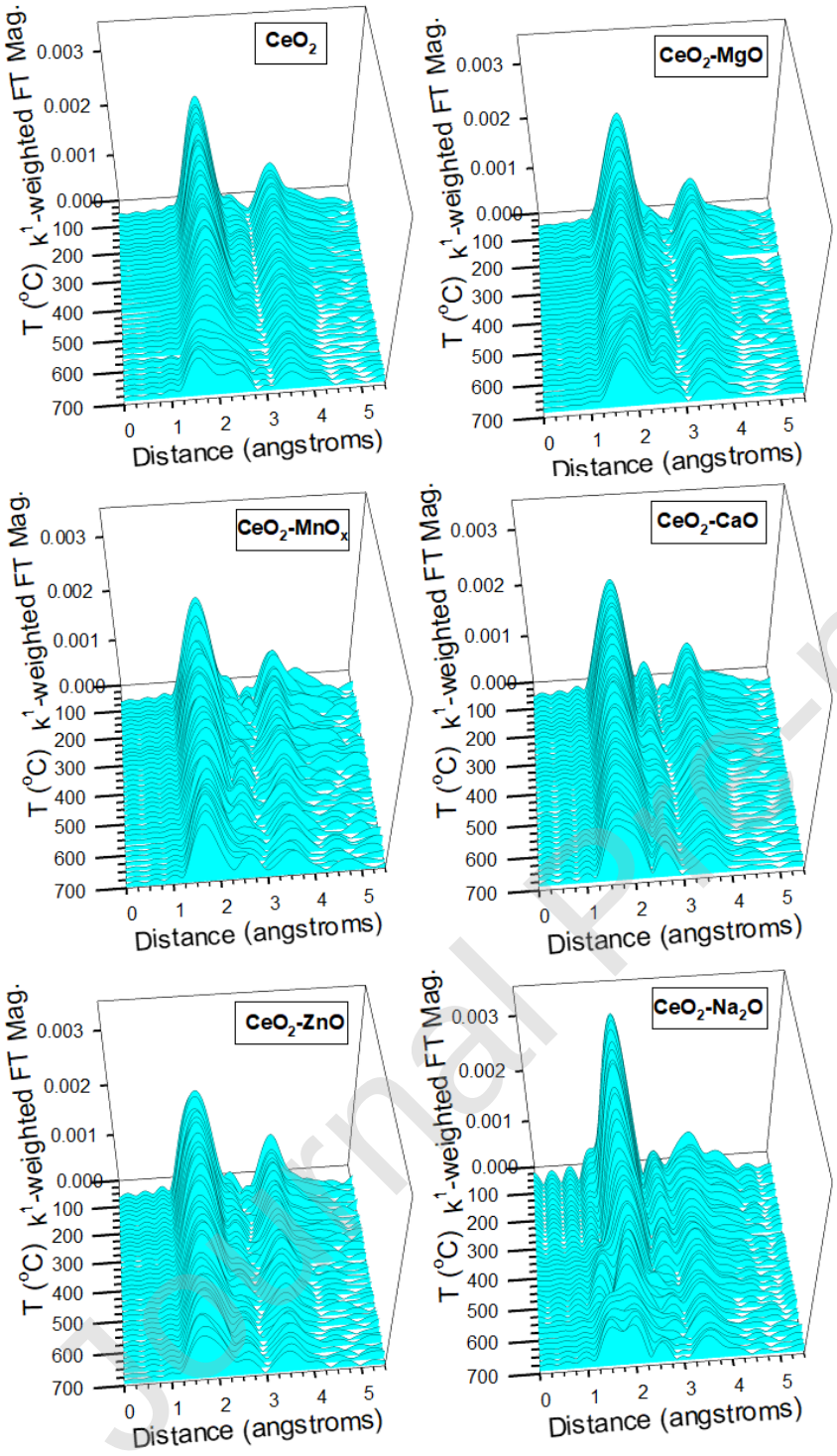

Fig. 4 H_2-TPR-EXAFS of spectra of CeO_2 and CeO_2-MeO_x catalysts.

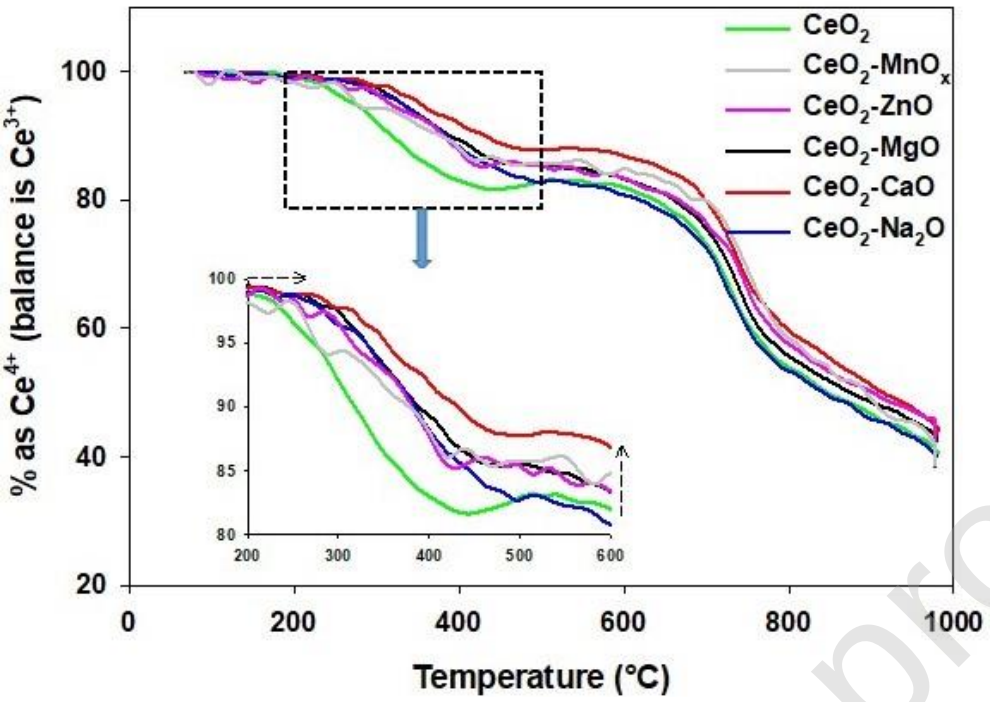

Fig. 5 Percentage of Ce^{4+} in the cerium component, balance Ce^{3+} along the TPR trajectory of CeO_2 and CeO_2-MeO_x catalysts.

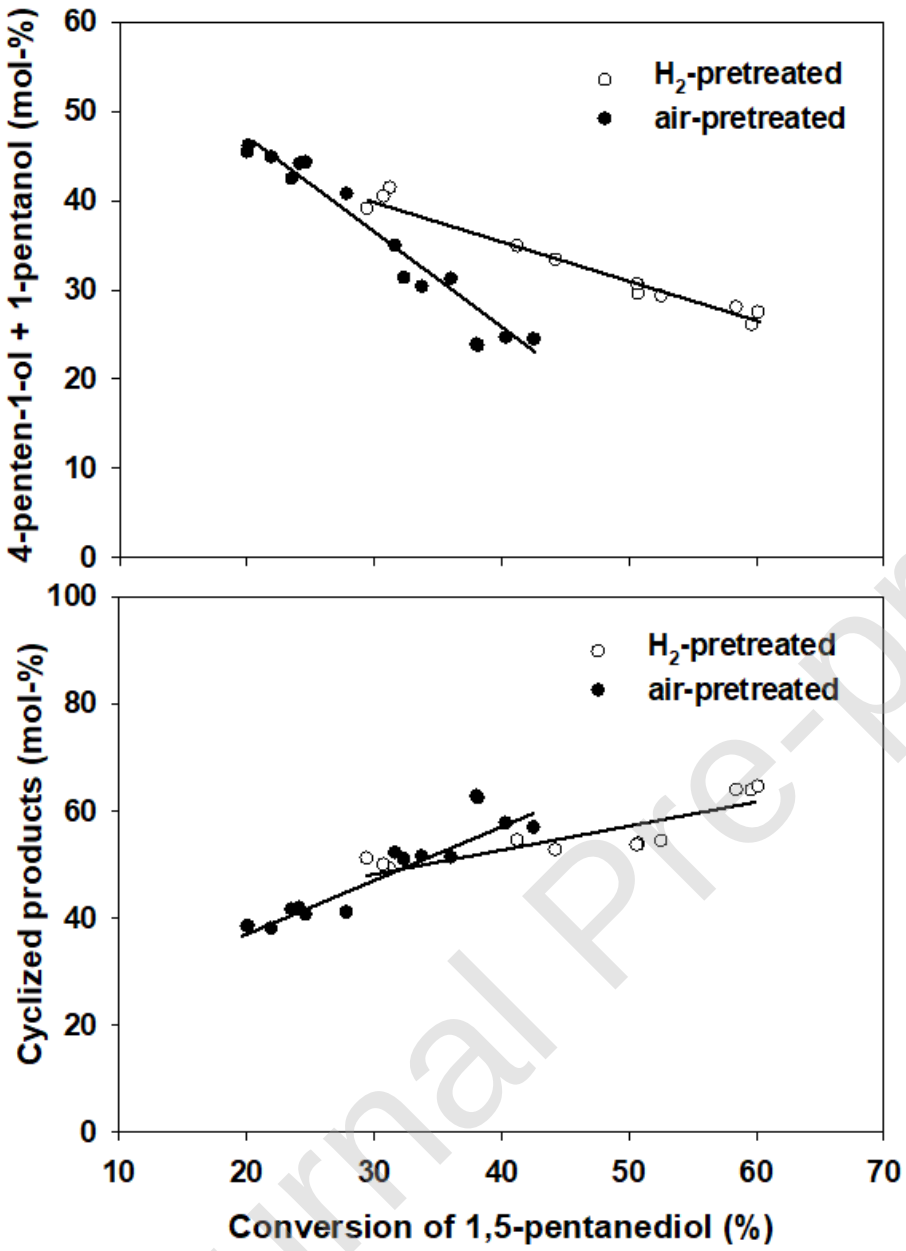

Fig. 6 The effect of conversion of 1,5-PDO on product selectivity

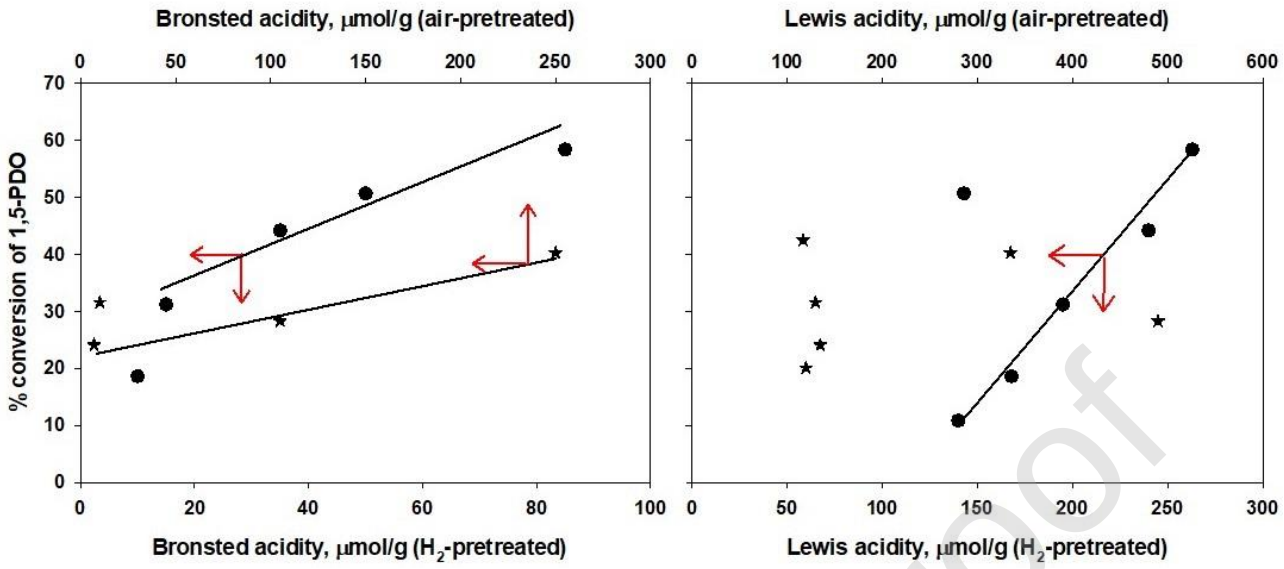

Fig. 7 The relationship between acidity and the conversion of 1,5-PDO on CeO_2 and CeO_2-MeO_x catalysts after different pretreatments

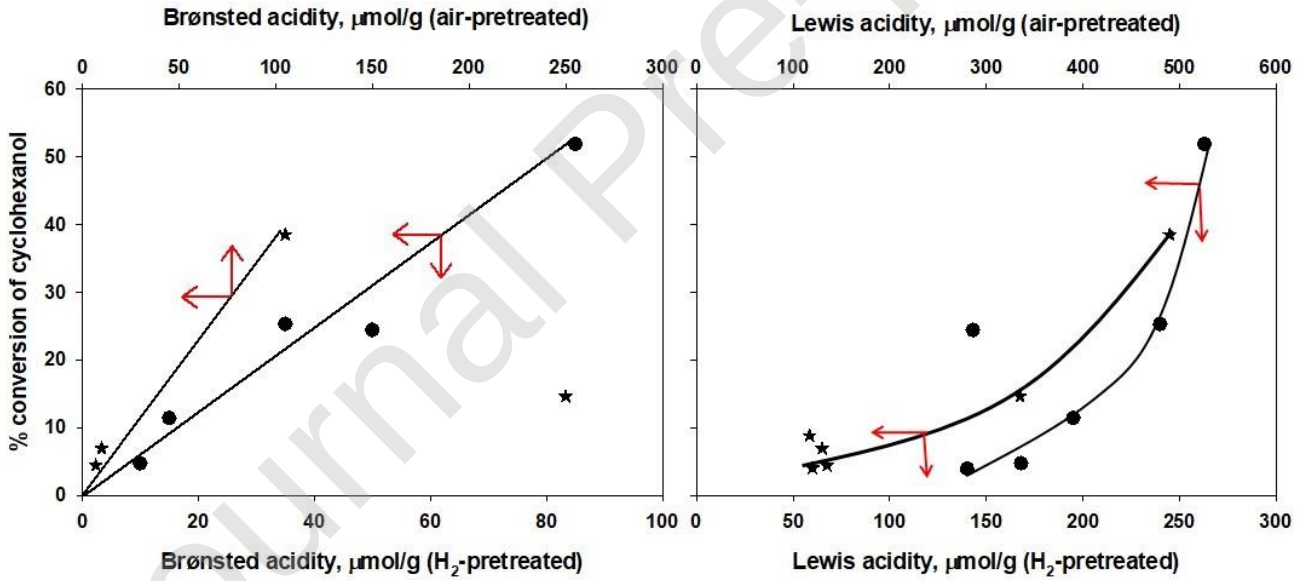

Fig. 8 The relationship between acidity and the conversion of cyclohexanol on CeO_2 and CeO_2-MeO_x catalysts after different pretreatments

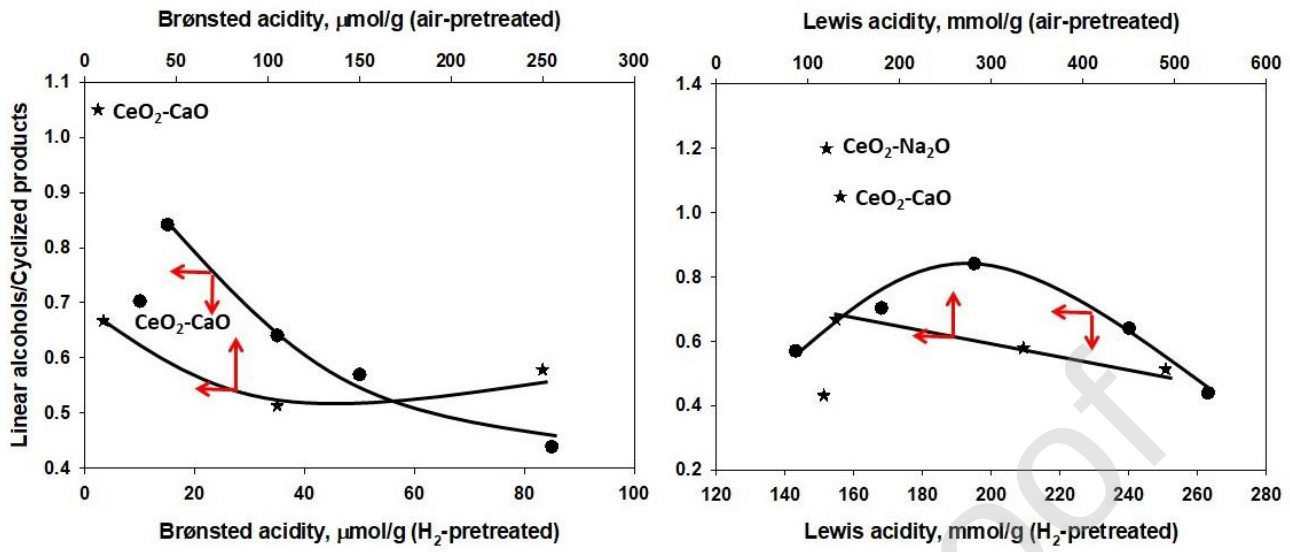

Fig. 9 The relationship between acidity and the ratio of linear alcohols/cyclized products on the conversion of 1,5-PDO on CeO_2 and CeO_2-MeO_x catalysts after different pretreatments

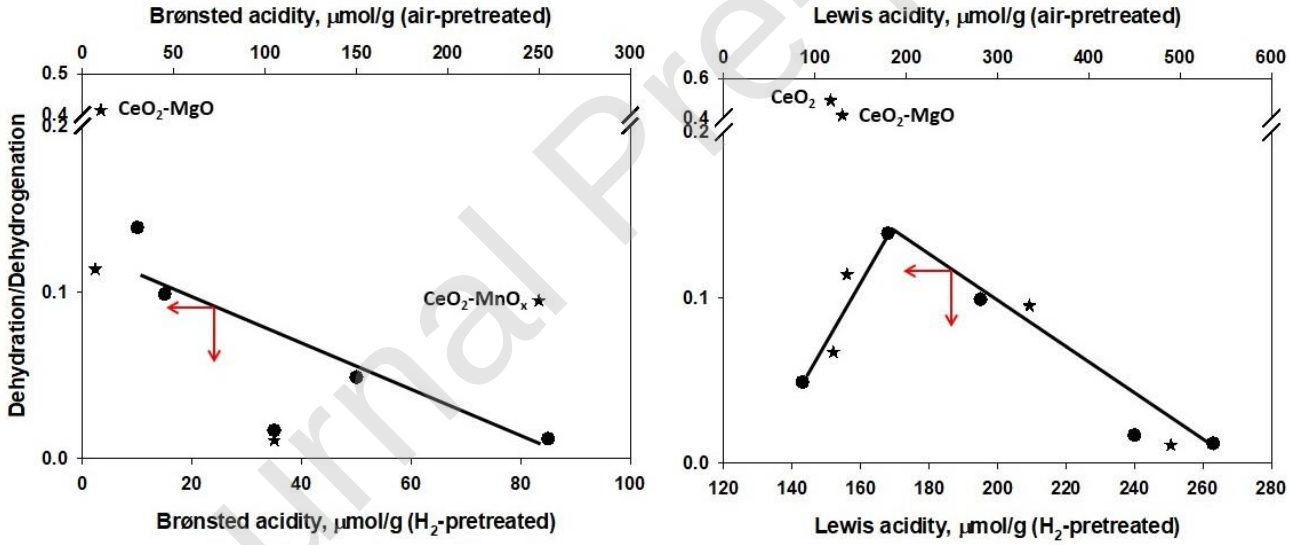

Fig. 10 The relationship between acidity and the ratio of dehydration/dehydrogenation for the conversion of cyclohexanol on CeO_2 and CeO_2-MeO_x catalysts after different pretreatments